Environmental Science
Processes & Impacts

Accepted Manuscript

ROYAL SOCIETY OF CHEMISTRY

rsc.li/process-impacts

Characterization and sources of black carbon in $PM_{2.5}$ at a site close to a roadway in Gwangju, Korea, during winter

Seung Shik Park[1,*] and Kwon-Ho Lee[2]

[1]*Department of Environment and Energy Engineering, Chonnam National University, 77 Yongbong-Ro, Buk-gu, Gwangju 500-757, Korea*

[2]*Department of Atmospheric & Environmental Sciences, Gangneung-Wonju National University, Korea*

*Author to whom correspondences should be addressed: Fax: 82-62-530-1859 e-mail: park8162@chonnam.ac.kr

Potential source contribution function maps for black carbon (BC) observed at a roadway site indicate that the BC observed during episode "A" was most likely attributed to local emissions, while local sources and regional transport of air masses contributed to the enhanced BC concentrations during episode "B".

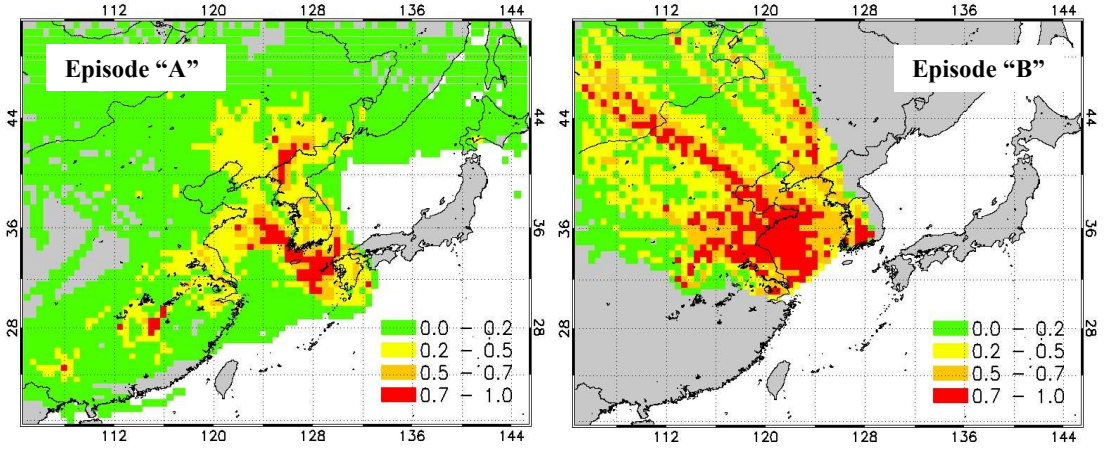

Abstract

Continuous measurements of black carbon (BC) concentrations in $PM_{2.5}$ were conducted using a single-wavelength aethalometer (@880nm, Magee Sci., AE16) at a site close to roadway (~70 m from roadside) in Gwangju, Korea, during winter (December–February) to investigate the character and sources of BC particles. The BC concentrations ranked in the order of January > December > February, probably due to lower boundary layer height, ambient temperature, and wind speed during January. Diurnal patterns in BC and carbon monoxide (CO) levels exhibited peak concentrations during the morning and evening hours coinciding with rush-hour traffic, with strong correlation (R^2) ranging from 0.52 (December) to 0.87 (January). It was found that wind speed was an important factor controlling BC concentrations at the site. Very high BC concentrations, up to ~18.0 $\mu g/m^3$, were observed at wind speeds <1.5 m/s. The BC concentrations acquired under weak wind conditions are highly correlated with CO with $\Delta BC/\Delta CO$ (the slope of BC and CO correlation) of 0.0063 (R^2=0.55, $p<0.01$) and 0.0065 (R^2=0.59, $p<0.01$) $\mu g/m^3$/ppbv during day and night, respectively, suggesting no significant difference in the fraction of diesel vehicles to total road traffic flows between the daytime and nighttime periods.

Two BC episodes, "A" and "B", were classified based on BC, $PM_{2.5}$, and secondary SO_4^{2-} concentrations, and discussed to investigate the difference in the evolution of the BC observed. Episode "A" was associated with high BC and low $PM_{2.5}$ and SO_4^{2-} concentrations, while episode "B" was associated with high concentrations of BC, $PM_{2.5}$, and SO_4^{2-}. Based on the temporal profiles of BC, NO, and NO_x concentrations, CO/NO_x ratio, and potential source contribution function map for BC, the BC observed during episode "A" was mostly attributed to locally produced emissions (e.g., traffic). However, the BC during episode "B" was influenced by long-range transport of air masses from China, as well as the local emissions.

Keywords: Black carbon, roadway site, $\Delta BC/\Delta CO$ ratio, potential source contribution function, long-range transport of air masses.

Environmental impact

Results from continuous measurements of BC concentrations at a roadway site during winter indicate that the diurnal cycles of BC were greatly influenced by boundary layer height, ambient temperature, and wind speed. Little difference in the slope of BC and CO correlation was found between day and night. BC episodes identified could be attributed to long-range transport of air masses, as well as the local emissions.

Introduction

Black carbon (BC) is an important species of particulate matter that results from the incomplete combustion of fossil fuels and biomass. BC plays an important role in Earth's climate system.[1-3] It has been estimated that global radiative forcing of BC aerosol is about +0.9 W/m^2 (+0.4 ~ +1.2 W/m^2), which makes it the second contributor to global warming after carbon dioxide.[4] Coated BC particles also act as cloud condensation nuclei (CCN), therefore contributing to the indirect forcing of the climate.[5] In addition to its impact on the climate system, BC has been linked to adverse health effects, including respiratory and cardiovascular diseases.[6-8] Once emitted, the BC aerosol can be transported over regional to synoptic scales, and removed from the atmosphere through wet and dry deposition.[9,10] Because of the shorter lifetime of BC in the atmosphere compared to carbon dioxide, reducing the BC emissions is an attractive option to mitigate global warming. However, the reduction of BC emissions may cause a decrease in CCN concentrations and a decrease in the indirect effect of aerosols, compensating for the decrease in the direct effect of BC.[11] Due to its potential impact on climate and human health, BC (or elemental carbon, EC) measurements have been conducted in urban and background sites in Korea to investigate the characteristics of the BC and to estimate its radiative forcing.[12-20] For example, Kim *et al*.[18] indicated that ambient BC over the Korean Peninsula was influenced by both long-range transport and local sources; urban areas (Seoul and Gwangju) have greater contributions to BC emissions from local sources while background areas (Gosan and Anmyeon Island) are dominated by long-range transport. Direct radiative forcing of BC over the Korean Peninsula was also estimated to be +0.1~+1.8 W/m^2 with the domain-average value of 0.39 W/m^2. However, few measurements of ambient BC in Korea have been conducted close to roadways where pedestrians and residents living near roads are often exposed to elevated particulate matter emissions from motor vehicles. Thus continuous measurements of BC near roadways are required for assessing the degree of human exposure and for developing traffic emission control strategies.

As discussed above, BC emission data are needed to assess their effects on health and climate. However, assessing BC emissions is difficult because of the high uncertainty in the fraction of total particulate matter that is BC (or EC) in particles ≤1.0 μm in diameter. The BC emissions vary significantly with vehicle fuel type (diesel vs. gasoline) and combustion conditions.[21-24] Therefore, an alternative methodology for assessing BC emissions, based on the relationship between ambient BC and CO, has been suggested.[13,25-31] According to the

previous studies, the slope of the BC-CO correlation (ΔBC/ΔCO) is a good parameter by which assess BC emissions and to distinguish different BC sources. It was suggested that ΔBC/ΔCO ratios are affected by the contribution of diesel vehicles to BC emissions to the total traffic flows.[31-33] Also, a higher ratio was observed at roadway sites than at urban and rural sites[31-34] and at night due to the higher proportion of heavy-duty diesel vehicles than during the day.[27,29,31] A higher ratio was also observed in summer than in winter due to the enhanced CO emissions in winter.[28,31]

In this study the results of hourly BC measurements close to a roadway in Gwangju, Korea during winter are presented. The temporal variations of BC are examined in the light of CO and meteorological parameters (boundary layer height, wind speed, and ambient temperature). The ΔBC/ΔCO from our continuous observations is derived and compared with the results from previous studies on roadways and urban sites. In addition, the difference in characteristics and sources of BC between two BC episodes classified based on concentrations of $PM_{2.5}$ and secondary SO_4^{2-} is discussed.

Experimental

Real-time measurements of BC

The site (35.11°N, 126.54°E) for real-time measurements of BC is about 70 m from a four-lane road in Gwangju, Korea, that carries heavy traffic, 0.5-0.6 km southwest of a major express highway, and surrounded by commercial and residential areas (Figure 1). Gwangju is situated in the southern part of Korea. It covers an area of 501.2 km^2 and has a population of 1.5 million people. In 2013 there were about 550,800 vehicles in Gwangju, 48.6% gasoline powered and 39.1% diesel powered. The latter includes cars and light- and heavy-duty trucks. About 85% of the total air pollution emissions in the city are attributed to vehicle sources. Pollution has usually been influenced by long-range transport of anthropogenic and natural aerosol particles from China.[35-37]

Continuous 5-min measurements of BC in $PM_{2.5}$ were made using a single-wavelength Aethalometer (@880nm, Magee Sci., AE16) between December 1, 2012 and February 28, 2013. Hourly average concentrations of $PM_{2.5}$, CO, NO, and NO_x were measured using an ambient air monitoring system from the Ministry of the Environment, at a location about 2.0 km from the roadside site. The recording of the CO data at the monitoring site was made with a resolution of 100 ppbv. Hourly concentration of SO_4^{2-} in $PM_{2.5}$ observed using an ambient ion monitor (AIM, URG9000D, URG Corporation) at an air pollution monitoring supersite ~7

km northwest of our sampling site, was also used as auxiliary data in this study. Details of the AIM monitor have been described by Park *et al.*[38]

Empirical compensation of aethalometer BC data

The operating principle of the Aethalometer is based on the measurement of the optical attenuation of a beam of light transmitted through a sample collected on a filter. It is assumed that the optical attenuation (ATN) only increases due to light absorption by the accumulation of BC on the filter.[39] Therefore, the BC concentration from the Aethalometer is determined by the rate of change of attenuation, as below:

$$BC_{uncorrected} = \frac{A \times \Delta ATN}{\sigma_{ATN} \times Q \times \Delta t} \qquad (1)$$

where A is the collecting spot area (cm^2), σ_{ATN} the optical absorption cross section ("specific attenuation") of BC (m^2/g), ΔATN is the change in attenuation during the time interval Δt, Q is the volumetric flow rate (l/min), and Δt is the sampling time (min). The specific attenuation coefficient used in this study was 16.6 m^2/g (@ λ=880nm), as recommended by the manufacturer.

However, results from previous studies indicated that as the ATN increases, the relationship between ATN change and BC concentration is not linear,[40-42] resulting in the underestimated BC. In order to correct the underestimation of BC, the compensation algorithm presented by Virkkula *et al.*[42] was used. The principle of the algorithm is briefly introduced below. The BC concentration is actually related to the absorption and attenuation coefficients by the following equation: $BC=b_{ATN}/\sigma_{ATN}$. The attenuation coefficient b_{ATN} (m^{-1}) may differ significantly from the true aerosol attenuation coefficient due to the particle loading effect on the filter matrix. The corrected BC concentration is calculated from the equation below:

$$BC_{corrected} = \frac{b_{ATN,corrected}}{\sigma_{ATN}} = (1 + k \cdot ATN) \cdot BC_{uncorrected} \qquad (2)$$

where k is an empirically derived constant. It was suggested that the particle loading effect varies with sampling locations, season, and aging degree of aerosols.[43,44] This approach has

also been applied in previous studies.[31,44,45] The magnitude of the particle loading effect could be larger in fresh darker aerosols than in aged aerosols mixed with optically scattering species,[40] and also larger in winter than in summer.[31] In this work, the *k* factor for December, January, and February was 0.0046, 0.0031, and 0.0032, respectively, suggesting a greater impact from fresh BC emissions in December than in other months.

Identification of source regions of BC using PSCF analysis

To identify the potential source locations of BC, the potential source contribution function (PSCF) was calculated using the concentrations of hourly BC data and backward trajectories data. The PSCF indicates the conditional probability that an air mass with a certain level of pollutant concentrations originated in a given grid cell.[14,46-48] A detailed description of PSCF analysis can be found elsewhere.[14] Briefly, the PSCF value for the grid cell is calculated by counting the trajectory segment endpoints that terminate within that grid cell. If the total number of end points that fall in the ij^{th} cell is n_{ij} and there are m_{ij} points for which the observed aerosol parameter exceeds a criterion value selected for this parameter, the PSCF value for the ij^{th} cell can then be defined as

$$PSCF_{ij} = m_{ij} / n_{ij} \qquad (3)$$

Four-day backward trajectories at heights of 100-1500 m above ground level (at 100m intervals) were calculated every 1 h during the BC pollution episodes identified (below) using the HYSPLIT 4.8 (Hybrid Single-Particle Lagrangian Integrated Trajectory) model,[49] so that the source regions of air masses reaching the sampling site (35°11′N, 126°54′E) for the pollution episodes could be identified. In order to down-weigh high PSCF values with high uncertainties in the cells with small values of n_{ij}, an arbitrary weight function, $W(n_{ij})$, was multiplied into the PSCF value to better reflect the uncertainty in the values for these cells.[46] The PSCF values were down weighted when the total number of end points per a particular cell was less than about three times the average value of the end points per each cell:

$$W(n_{ij}) = \begin{cases} 1.0 & 48 \le n_{ij} \\ 0.7 & 5 < n_{ij} \le 48 \\ 0.5 & 2 < n_{ij} < 5 \\ 0.2 & n_{ij} \le 2 \end{cases} \qquad (4)$$

Results and Discussion

$PM_{2.5}$ BC concentrations

Figure 2 shows the time series of 1-hr averaged BC concentrations over the measurement period. The temporal profiles of hourly $PM_{2.5}$ and SO_4^{2-} concentrations are also shown in Figure 2. The hourly average BC concentration was 2.4±2.2 (0.2-17.9) μg/m^3. The monthly average BC concentration was 1.9±1.9 μg/m^3 in December, 3.0±2.8 μg/m^3 in January, and 2.1±1.5 μg/m^3 in February. Comparison of temporal profiles of BC and $PM_{2.5}$ concentrations indicates that typically an increase in BC leads to an increase in $PM_{2.5}$ concentration. However, although $PM_{2.5}$ concentration was observed to be low, extremely high BC concentration (up to ~17.9 μg/m^3) occurred between December 13 and 16, 2012. During this period, hourly $PM_{2.5}$ ranged from 17 to 51 μg/m^3. In this study, two BC episodes were classified based on BC, $PM_{2.5}$, and SO_4^{2-} concentration levels to investigate the difference in evolution of BC between the two episodes. The first episode (episode "A") observed between December 13 and 16, 2012, is associated with a high BC and low $PM_{2.5}$ and SO_4^{2-} (1.4-9.3 μg/m^3). The second episode (episode "B") observed between January 10 and 16, 2013, is strongly related to high concentrations of BC, $PM_{2.5}$ (up to 127 μg/m^3), and SO_4^{2-} (1.1-25.3 μg/m^3), and also with severe regional haze lingering over northeastern China.[50,51] Detailed discussion on the two BC episodes is below given.

Figure 3 shows the average diurnal BC concentration measured in December, January, and February. Diurnal variations of CO, boundary layer height (BLH), ambient temperature, and wind speed are also included in Figure 3. In this work, the hourly BLH in Gwangju are determined by 1) morning and afternoon estimates of BLHs; 2) the local standard time (LST) of sunrise and sunset; and 3) hourly estimates of stability. Morning and afternoon BLH estimates were based on the algorithm described by Holzworth.[52] Briefly, in order to compute the morning BLH, the minimum temperature is determined from 00:00 through 08:00 LST. The morning BLH was estimated as the height above ground at which the dry adiabatic extension of the morning minimum surface temperature plus 5 intersects the vertical temperature profile observed at 12:00 GMT. A similar computation for the afternoon BLH was made using the maximum surface temperature observed from 12:00 through 17:00 LST. Hourly BLHs are interpolated from these twice per day estimates. As shown in Figure 3, strong diurnal patterns were observed with peak concentrations of 2.6, 5.4, and 3.2 μg/m^3 at 08:00-09:00 in December, January, and February, respectively. The BC concentrations were

observed to be the lowest at midday. The evening peaks occurred between 19:00 and 22:00 depending on the month. Diurnal BC was highly correlated with CO with R^2 of 0.52, 0.87, and 0.82 in December, January, and February, respectively, suggesting their impact from common sources, e.g., traffic emissions. The abundance of BC with time in the urban atmosphere is influenced not only by combustion activities, but also by dispersion condition. Typically, BC has a tendency to decrease when traffic emissions are reduced. As shown in Figure 3(c), boundary layer height in February was higher than in December and January, indicating a larger dilution effect of air pollutants in February. The higher boundary layer height in February than in other months is attributed to higher ambient temperature, which enhances convective activity. The development of a well-mixed layer height started at 08:00, reached maximum values around 13:00, and decreased after 17:00. Traffic congestion, along with stable atmospheric conditions with low mixing layer heights during the morning and evening hours, may result in significantly enhanced BC concentrations. The dilution effect resulting from the development of the planetary boundary layer during the day prevented the BC concentrations from becoming very large. Also, for the measurement period, higher wind speeds have a strong dilution effect on BC concentrations during the daytime (Figure 3(e)). However, this is no longer the case just before sunrise and after sunset, when the combination of dense traffic and a low boundary layer is responsible for the observed sharp increase in BC concentration, as shown in Figure 3(a). The morning peak of BC was attributed to the combined effect of traffic emissions and lower mixing layer height and wind speed. The surface inversion after sunset resulted in the accumulation of BC, causing increased BC concentrations in the evening. Similar BC diurnal trends have been found at other urban sites.[29,44,53-55] On a monthly basis, diurnal ambient temperatures and wind speeds in January were lower than those in December and February, suggesting that ambient temperature and wind speed could be possible factors to the increased diurnal BC concentrations in January. Also long-range transport of BC aerosol from northeastern China[50,51] was likely another cause of the enhanced BC concentrations in January at the site. This is clearly supported by PSCF result for BC (see Figure 9).

Impact of wind speed and wind direction on BC concentrations

Meteorological parameters play important roles in determining the concentration levels of air pollutants in urban areas.[29] Among the meteorological parameters, wind speed is an important factor controlling the BC concentrations.[54,56,57] The dependence of BC concentration on local wind speed is shown in Figure 4. In order to investigate the impact of wind speed on BC,

winds were divided into eight categories based on speed: 0-1.0, 1.0-1.5, 1.5-2.0, 2.0-2.5, 2.5-3.0, 3.0-3.5, 3.5-4.0, and >4.0 m/s. Very high BC concentrations were observed at wind speeds <1.5 m/s, suggesting accumulation of BC under poor dispersion conditions. As the wind speed increases, BC concentrations exhibited a gradually decreasing trend due to stronger BC dispersion (R^2=0.92, p<0.0001). Therefore, accumulation under weak wind conditions and a strong dilution effect in the daytime suggests the predominance of local sources in increased BC concentrations. Similar results were obtained at other urban sites.[55,58,59] Figure 5(a) shows the directionalities of hourly BC concentrations at wind speeds >1.0 m/s. Since the identification of a source location is not well determined at low wind speeds, the BC data obtained at wind speeds <1.0 m/s were excluded from the analysis. As shown in Figure 5(a), hourly BC concentrations from wind directions of 20-50° and 220-250°, i.e. directions in which the Honam express highway and local traffic roads, respectively, are located (see Figure 1), were higher than those from other wind directions, indicating that higher BC concentrations from the wind sectors were likely due to the influence of road traffic emissions.

A conditional probability function (CPF) was utilized to identify likely locations of local emission sources affecting concentrations of BC at our measurement site. BC data obtained at wind speeds < 1.0 m/s were excluded in the CPF calculation. Figure 5(b) shows the CPF concentration plots of BC when the 75th percentile of their concentrations was set as the threshold criterion. The emission sources are likely located in the directions that have high conditional probability values. The CPF plot for the BC data indicates the major BC contributions to the site coming from wind directions between 60 and 90° and between 210 and 240°. However, due to a very low frequency (<1%) observed when winds blew from the direction of 60-90°, it is suggested that sources could likely be from the southwesterly (210-240°) emissions, i.e., road traffic emissions, which is similar to the directionality of BC shown in Figure 5(a).

Correlation between BC and CO concentrations

It has been found that BC and CO in urban sites are strongly correlated since road traffic activity is a major source of both BC and CO.[12,13,27,29,30,31] The emission ratios of BC/CO can vary significantly with the type of combustion source and the age and condition of the vehicle fleet.[21,22] For example, the BC/CO ratios are known to be much higher in emissions from diesel engines than those from gasoline engines. Therefore the BC/CO ratios can be used to

distinguish the various sources. Previous studies in urban sites also suggest that atmospheric BC concentrations are predominantly controlled by emissions from heavy-duty diesel vehicles.[28,29,31] In addition, BC emissions have been found to be significant from gasoline-powered vehicles under certain conditions, such as cold-start ignition, hard acceleration, and fuel-rich combustion.[23,60] Figures 6(a)-6(b) show the correlations between BC and CO for daytime and nighttime periods. In this study, daytime was defined as the hours between sunrise (07:00) and sunset (17:00) and nighttime as from just after sunset to just before sunrise. Only the BC data acquired at wind speeds ≤2.0 m/s were selected because air pollutants are more homogeneously distributed across the road and likely to be associated with local emissions rather than long-range transport.[61] Also for further perspective, the ΔBC/ΔCO (the slope of BC and CO correlation) ratio derived from this study is compared with the results reported for other urban areas (Table 1). As shown in Figure 6, the BC concentrations were well correlated with CO during daytime and nighttime with R^2 of 0.55 and 0.59, respectively, suggesting the influence of two species from common sources, i.e., motor vehicles. EC is known to be correlated with CO in other urban areas as well,[12,13,26,29] because both species are emitted from the incomplete combustion of fossil fuels. The correlation slope of ΔBC/ΔCO using all data at wind speeds ≤2.0 m/s was 0.0064 μg/m^3/ppbv (R^2=0.57). The ΔBC/ΔCO ratio in this study is comparable to, or greater than those at the roadside and urban sites (Table 1). The ΔBC/ΔCO ratio (unit in μg/m^3/ppbv) was 0.0056 in three sites in Tijuana, Mexico,[30] 0.0047-0.0090 at a roadside site in Beijing, China,[31] 0.0054-0.0079 in Guangzhou, China,[29,53] 0.0035-0.0058 in Beijing, China,[28] 0.0058 in regional and urban industrial emissions from Dallas and Houston, USA,[62] 0.001 in Mexico city, Mexico,[63] and 0.0057 in Tokyo and 0.0063 in Nagoya, Japan.[27] It was demonstrated that the ΔBC/ΔCO ratios at roadway sites were typically higher due to considerable emissions from road traffic, than those at the urban and rural sites.[31-34] Also, as the fraction of heavy-duty diesel vehicles (HDDVs) near the roadside site increases, the ratio had a tendency to increase. Results from previous urban measurements indicated higher ratios in summer than in winter,[28,31] and higher during the night than during the day at the roadside site due to a much higher proportion of HDDVs during the night.[27,31] These results are expected because traffic emissions are an important source of BC and CO in these urban regions. However the ΔBC/ΔCO ratio in this study was 0.0063 μg/m^3/ppbv (R^2=0.55) during the day and 0.0065 μg/m^3/ppbv (R^2=0.59) during the night, suggesting no significant difference in the contribution of diesel vehicles to BC emissions from total road traffic flows between the day and the night. As shown in Figure

3(f), the diurnal variation of the ΔBC/ΔCO ratios was similar to those of BC and CO, with morning and evening peaks. The decrease in BC to a large extent in the afternoon is related to the decrease in CO (see Figure 3(a) and (b)), leading to the decreased ΔBC/ΔCO ratio in the afternoon. Considering that BC/CO emission ratios for vehicles are lower under the cold conditions,[27,28] the higher ΔBC/ΔCO ratio in February than in other months (Figure 3(f)) is due to the decreased CO emissions with increasing ambient temperature (see Figure 3(b) and (d)). Generally, the ΔBC/ΔCO ratios are considered as a gauge of the fraction of diesel vehicles to all the types of vehicles because CO emissions are dominated by gasoline vehicles while BC is mostly emitted from diesel vehicles. Thus, emission factors and traffic densities of gasoline and diesel vehicles are necessary to better understand the diurnal cycles of the ΔBC/ΔCO ratios at the study site. Average BC and CO concentrations were 3.1 μg/m^3 and 869 ppbv for the weekdays and 2.6 μg/m^3 and 797 ppbv for the weekends, respectively. The BC correlates well with CO during the weekdays with a slope of 0.0065 μg/m^3/ppbv and an R^2 of 0.54, and during the weekends with a slope of 0.0071 μg/m^3/ppbv and an R^2 of 0.68. T-test for the BC/CO ratio indicates also that the BC/CO ratios were not statistically different between the weekdays and weekends ($p > 0.05$).

Investigation on the origin of BC during two episodes

Two BC pollution episodes were discussed to investigate the difference in the evolution of observed BC. Figure 7 shows temporal variations of hourly BC, wind speed, NO, and NO_x for two episodes. The relationship between NO/NO_x and CO/NO_x is also shown. In addition, temporal profiles of hourly SO_4^{2-} and NO_3^- concentrations, SOR, and NOR are shown in Figure 8. SOR and NOR indicate the sulfur oxidation ratio ($=SO_4^{2-}/(SO_4^{2-}+SO_2)$) and nitrogen oxidation ratio ($=NO_3^-/(NO_3^-+NO_2)$), respectively, and may be used to estimate the contribution of SO_4^{2-} and NO_3^- formation from SO_2 and NO_2.[38,66] The PSCF maps for BC for two episodes are shown in Figure 9.

The hourly ambient temperature ranged from -4.5 to 11.5℃ during episode "A" and from -7.3 to 7.3℃ during episode "B". The respective average relative humidity (RH) was 77.5% (36.0-98.0%) and 66.3% (28.0-94.0%). High RH for episode "A" was attributed to rain on December 14. It started raining at 07:00 and stopped at 21:00 (RH=95-98%) on December 14 with a precipitation of 23 mm. Wind speeds, for the periods when BC concentrations were relatively enhanced, were mostly <1.0 m/s and <1.3 m/s for episodes "A" and "B", respectively. The relatively low wind speed and temperature during the two BC episodes may

account for the higher accumulation of locally emitted air pollutants and the enhanced formation of secondary aerosols. In addition, the high RH in episode "B" under no rain conditions would accelerate the aqueous phase oxidation of secondary aerosols, which resulted in increased SO_4^{2-} and NO_3^- concentrations. As shown in Figure 6(c) and 6(d), the $\Delta BC/\Delta CO$ slope was 0.0076 (R^2=0.74) and 0.0061 μg/m^3/ppbv (R^2=0.71) during episodes "A" and "B", suggesting no significant difference in the $\Delta BC/\Delta CO$ slope between the two episodes, but a lower slope in episode "B" was likely attributed to both low contribution of diesel vehicles to BC emissions and long-range transport of combustion emissions from northeastern China (see Figure 9). The BC/CO ratio during the transport decreases due to the shorter lifetime of BC compared to CO, resulting in the decrease in $\Delta BC/\Delta CO$ ratio during episode "B".

Diurnal BC peak concentrations over the two episodes occurred during morning and evening rush-hour periods. As the boundary layer rose throughout the morning and early afternoon, the BC concentrations tended to decrease. Close inspection of Figure 7 revealed low BC background levels during episode "A" with values of 0.5-1.5 μg/m^3. During episode "B", BC concentration exceeding 4.0 μg/m^3 lasted about 4 days and relatively high BC background levels were maintained. The temporal profile of BC concentration for episode "B" exhibited a continuous increase in the BC background level from 0.5-1.0 μg/m^3 on January 11 to 2.5-4.0 μg/m^3 from January 12 through 15, probably due to long-range transport of polluted air masses (see PSCF map in Figure 9) and air stagnation conditions. The highest BC concentrations during episodes "A" and "B" were 17.9 and 15.7 μg/m^3, respectively, which were observed on the evening of December 14 and in the morning of January 12. As shown in Figure 7, temporal variations of BC throughout the episodes were quite similar to those of NO, which is a primary species from combustion sources, with R^2 of 0.79 and 0.62, respectively. For the time period when BC concentration peaked, NO and NO_x for episodes "A" and "B" were 390 and 481 ppbv, and 193 and 270 ppbv, respectively, indicating NO/NO_x of 0.73 and 0.71. Respective NO/NO_x was in the range of 0.63-0.81 and 0.48-0.73. Both high NO/NO_x and a strong correlation of BC with NO suggest that the BC observed during the two BC episodes was significantly associated with locally produced emissions. In order to further examine the influence of local emissions on the two BC episodes, the NO/NO_x against the CO/NO_x was shown in Figure 7. Previous studies have indicated that CO/NO_x could be used to examine the evolution of the aerosol chemical composition with respect to the age of the air masses as a proxy for proximity to major pollution sources and atmospheric processing.[38,67,68]

For example, CO/NO_x ratios of 5–15, 10–50, and >50 were classified as urban, near-source and aged regional conditions, respectively. As shown in Figure 7, the NO/NO_x for episodes "A" and "B" decreased exponentially with increasing the CO/NO_x with R^2 of 0.67 and 0.52, respectively. The respective CO/NO_x was in the range of 8-40 and of 8-80. The R^2 value and CO/NO_x suggest that the BC aerosols observed during episode "A" were more influenced by local emissions (urban + near sources) than those during episode "B".

As shown in Figure 8, higher concentrations of SO_4^{2-} and NO_3^- were observed during episode "B" than episode "A". SO_4^{2-} and NO_3^- concentrations were 3.3 (1.4-9.3) and 6.3 (2.5-11.6) $\mu g/m^3$ during episode "A" and 9.9 (1.1-25.3) and 12.1 (1.0-31.1) $\mu g/m^3$ during episode "B", respectively. Also higher SOR and NOR ratios were observed in episode "B". SOR and NOR were 0.21 (0.09-0.37) and 0.11 (0.04-0.26) during episode "A" and 0.29 (0.10-0.53) and 0.14 (0.03-0.36) during episode "B", respectively, indicating further oxidation of the aerosols collected for episode "B". Results of t-test for SOR and NOR indicate that the SOR ($p < 0.001$) and NOR ($p < 0.01$) were statistically different between the episodes. The PSCF map for BC for episode "A" shows clearly the influence of local emissions, while the PSCF map for BC during episode "B" indicates that the long-range transport of air pollutants over northeastern China could be one possible source of BC and secondary inorganic species observed for episode "B", as well as the local emissions.

In summary, the majority of the BC observed during episode "A" originated locally, while the BC observed during episode "B" could reflect long-range transported aerosols, as well as local emissions.

Summary and Conclusions

To investigate the characteristics and sources of BC particles, 5-min integrated BC concentration was observed with a single-wavelength Aethalometer at a site close to a roadway in Gwangju, Korea, during winter (December 2012 through February 2013). BC and CO concentrations peaked during the morning and evening coinciding with rush-hour traffic and their magnitude was influenced by meteorological parameters, such as boundary layer height, wind speed, and ambient temperature. The BC concentrations observed under weak wind conditions (wind speed ≤2 m/s) were highly correlated with CO mixing ratios with a $\Delta BC/\Delta CO$ ratio of 0.0063 (R^2=0.55, p<0.01) and 0.0065 $\mu g/m^3$/ppbv (R^2=0.59, p<0.01) for daytime and nighttime periods, respectively, suggesting no big difference in the fraction of

diesel vehicles to total road traffic flows between day and night. The slopes of ΔBC/ΔCO in winter at the study site were comparable to or greater than those in previous studies.

Two BC episodes, "A" and "B" over the entire study period, were classified based on BC, $PM_{2.5}$, and secondary SO_4^{2-} concentrations. BC background levels were observed to be low (0.5-1.5 μg/m^3) during episode "A" and high (2.5-4.0 μg/m^3) during episode "B", suggesting the influence of long-range transport of polluted air masses and/or air stagnation conditions during the episode "B" period. Close examination of temporal profiles of BC, NO, NO_x, and wind speed, relationship between NO/NO_x and CO/NO_x, sulfur oxidation ratio, nitrogen oxidation ratio, and PSCF maps for BC indicate that the BC observed during episode "A" was most likely attributed to local emissions rather than regional contributions, while local sources and regional transport of air masses contributed to the enhanced BC concentrations during episode "B".

Acknowledgement

This study was financially supported by Chonnam National University, 2014, and also supported by Basic Science Research Programs through the National Research Foundation of Korea (NRF) funded by the Ministry of Education (NRF-2014R1A1A4A01003896).

References

1 R.J. Charlson et al., *Science*, 1992, **255**, 423-430.
2 H. Horvath, *Atmos. Environ.*, 1993, **27A**, 293-317.
3 G. Myhre, A. Myhre and F. Stordal, *Atmos. Environ.*, 2001, **35**, 2361-2373.
4 V. Ramanathan and G. Carmichael, *Nature Geosci.*, 2008, **1**, 221–227.
5 C.H. Twohy and M. R. Poellot, *Atmos. Chem. Phys.*, 2005, **5**, 2289–2297.
6 K.L. Jansen et al., *Environ. Health Perspect.*, 2005, **113**, 1741–1746.
7 S.F. Suglia, A. Gryparis, R.O. Wright, J. Schwartz and R.J. Wright, *Am. J. Epidemiol.*, 2008, **167**, 80–286.
8 M.C. Power et al., *Environ. Health Perspect.*, 2011, 119, 682-687.
9 J.H. Seinfeld and S.N. Pandis, Atmospheric Chemistry and Physics: from Air Pollution to Climate Change, second ed. John Wiley & Sons, Inc, New York, USA, 2006.
10 T.C. Bond et al., *J. Geophys. Res.*, 2013, **118**, 5380–5552.
11 W.T. Chen et al., *Geophys. Res. Lett.*, 2010, **37**, L09801 doi:09810.01029/02010GL042886.
12 S.S. Park and Y.J. Kim, *Atmos. Environ.*, 2004, **38**, 1459-1471.
13 S.S. Park et al., *Atmos. Environ.*, 2005, **39**, 5101-5112.
14 S.S. Park et al., *Atmos. Res.*, 2008, **89**, 48-61.
15 Y.J. Kim, M.J. Kim, K.H. Lee and S.S. Park, *Atmos. Environ.*, 2006, **40**, 4064-4075.
16 K.J. Moon, J.S. Han and S.Y. Cho, *Asian J. Atmos. Environ.*, 2013, **7**, 129-138.
17 E.A. Stone, S.-C. Yoon and J.J. Schauer, *Aerosol Air Qual. Res.*, 2011, **11**, 31–43.
18 M.Y. Kim et al., *Atmos. Environ.*, 2012, **58**, 45-55
19 S. Lee et al., *Atmos. Environ.*, 2012, **50**, 246-254.
20 A.S. Panicker et al., *Atmos. Environ.*, 2013, **77**, 98-104.
21 T.W. Kirchstetter, R.A. Harley, N.M. Kreisberg, M.R. Stolzenburg and S.V. Hering, *Atmos. Environ.*, 1999, **33**, 2955-2968.
22 D. Baumgardner et al., *J. Geophys. Res.*, 2002, **107(D21)**, 8342, doi:10.1029/2001JD000626.
23 M.J. Kleeman, S.G. Riddle, M.A. Robert and C.A. Jakober, *Environ. Sci. Technol.*, 2008, **42**, 235-242.
24 D. Westerdahl, X. Wang, X. Pan and K.M. Zhang, *Atmos. Environ.*, 2009, **42**, 697-705.
25 L.-W. Chen et al., *Geophys. Res. Lett.*, 2001, **28**, 1711– 1714.
26 S.S. Park, D. Harrison, J. P. Pancras and J. M. Ondov, *J. Geophys. Res.*, 2005, **110**, D07S06, doi:10.1029/2004JD004610.
27 Y. Kondo et al., *J. Geophys. Res.*, 2006, **111**, D12205, doi:10.1029/2005JD006257.
28 S. Han et al., *J. Geophys. Res.*, 2009, **114**, D23202, doi:10.1029/2009JD012027.
29 R.L. Verma et al., *Atmos. Chem. Phys.*, 2010, **10**, 6471-6485.
30 C.A. Shores et al., *Atmos. Environ.*, 2013, **70**, 490-499.
31 S. Song et al., *Atmos. Environ.*, 2013, **77**, 213-221.
32 Y.F. Zhu, W.C. Hinds, S. Kim and C. Sioutas, *J. Air Waste Manage. Assoc.*, 2002, **52**, 1032-1042.
33 Y.F. Zhu, W.C. Hinds, S. Kim and C. Sioutas, *Atmos. Environ.*, 2002, **36**, 4323-4335.
34 C. Reche et al., *Atmos. Chem. Phys.,* 2011, **11**, 6207-6227.
35 H.L. Lee, S.S. Park, K.W. Kim Y.J. Kim, *Atmos. Res.,* 2008, **88**, 199-211.
36 S.S. Park and S.Y. Cho, *Aerosol Air Qual. Res.,* 2013, **13**, 1019-1033.
37 C.S. Son and S.S. Park, *Environ. Science: Processes & Impacts*, 2015, **17**, 561-569.
38 S.S. Park, S.A. Jung, B.J. Gong, S.Y. Cho and S.J. Lee, *Aerosol Air Qual. Res.*, 2013, **13**, 957-976.
39 A. Hansen, H. Rosen and T. Novakov, *Sci. Total Environ.*, 1984, **36**, 191-196.
40 E. Weingartner, H. Saathoff, M. Schnaiter, N. Streit, B. Bitnar and U. Baltensperger, *J. Aerosol Sci.*, 2003, **34**, 1445-1463.
41 W. Arnott, K. Hamasha, H. Moosmuller, P. Sheridan and J. Ogren, *Aerosol Sci. Technol.*, 2005, **39**, 17-29.
42 A. Virkkula et al., *J. Air Waste Manage. Assoc.*, 2007, **57**, 1214-1222.
43 J.R. Turner, *Epidemiology*, 2008, **19**, S65.
44 S.S. Park, A.D.A. Hansen and S.Y. Cho, *Atmos. Environ.*, 2010, **44**, 1449-1455.
45 Y.G. Wang et al., *Environ. Sci. Technol.*, 2011, **45**, 7387-7393.
46 A.V. Polissar, P.K. Hopke and J.M. Harris, *Environ. Sci. Technol.*, 2001, **35**, 4214-4226.

47 Y.Q. Wang, X.Y. Zhang and R. Arimoto, *Sci. Total Environ.*, 2006, **368**, 875-883.
48 S.S. Park et al., *J. Korean Soc. Atmos. Environ.*, 2013, **29(5)**, 642-655. (in Korean with English abstract)
49 R.R. Draxler and G.D. Rolph, HYSPLIT (HYbrid Single-Particle Lagrangian Integrated Trajectory) Model access via NOAA ARL READY Website (http://ready.arl.noaa.gov/HYSPLIT.php). NOAA Air Resources Laboratory, Silver Spring, MD, 2014.
50 X. Wang et al., *Sci. Total Environ.*, 2014, **493**, 133-137.
51 S. Park, S.Y. Cho and M.-S. Bae, *Sci. Total Environ.*, 2015, http://dx.doi.org/10.1016/j.scitotenv.2015.07.004.
52 G.C. Holzworth, *Mixing heights, wind speeds, and potential for urban air pollution throughout the contiguous*; United States. AP-101; U.S. EPA: Research Triangle Park, NC, 1972.
53 M.O. Andreae, O. Schmid, H. Yang et al., *Atmos. Environ.*, 2008, **42**, 6335–6350.
54 A. Saha and S. Despiau, *Atmos. Res.,* 2009, **92**, 27-41.
55 X. Chen et al., *Atmos. Pollut. Res.*, 2014, **5**, 361-370.
56 L.K. Sahu, Y. Kondo, Y. Miyazaki, P. Pongkiatkul and N.T.K. Oanh, *J. Geophys. Res.*, 2011, **116**, D15302.
57 Y.G. Wang, P.K. Hopke, O.V. Rattigan and Y.F. Zhu, *J. Environ., Monit.*, 2011, **13**, 1919-1926.
58 S. Ramachandran and T.A. Rajesh, *J. Geophys. Res.*, 2007, **112**, D06211, doi:10.1029/2006JD007488.
59 J.J. Cao et al., *Atmos. Res.*, 2009, **94**, 194-202.
60 M.A. Robert, S. VanBergen, M.J. Kleeman and C.A. Jakober, *J. Air Waste Manage. Assoc.*, 2007, **57**, 1414-1428.
61 J. Kukkonen et al., *Atmos. Environ.*, 2003, **37**, 1101-1112.
62 J.R. Spackman et al., *Geophys. Res. Lett.*, 2008, **35**, L19816.
63 D. Baumgardner, G.L. Kok and G.B. Raga, *Atmos. Chem. Phys.*,2007, **7**, 2517-2526.
64 K.M. Latha and K.V.S. Badarinath, *Atmos. Res.*, 2004, **71**, 265-274.
65 G. McMeeking et al., *Atmos. Chem. Phys.* 2010, **10**, 9393–9414.
66 X.J. Zhao et al., *Atmos. Chem. Phys.*, 2013, **13**, 5685-5696.
67 E.J. Freney et al., *Atmos. Chem. Phys. Discuss.,* 2011, **11**, 27139-27170.
68 W.T. Morgan et al., *Atmos. Chem. Phys.*, 2010, **10**, 4065-4083.

Table 1. Comparison of ΔBC/ΔCO ratios with other urban regions

Location	Sampling period	EC or BC ($\mu g/m^3$)	ΔBC/ΔCO ($\mu g/m^3$/ppbv)	Analytical method	Reference
Tokyo, Japan	May 2003 - Feb. 2005	1.9	0.0057	TOT	Kondo et al.[27]
Nagoya, Japan	March 2003	-	0.0063	Light absorption	Kondo et al. [27]
Gwangju, Korea	November 1999	7.2	0.0050	Light absorption	Park and Kim[12]
	March - May 2001	5.7	0.0060	TOT	Park et al.[13]
Guangzhou, China	July 2006	4.7	0.0054	TOT	Verma et al.[29]
	Oct. - Nov. 2004	7.1	0.0079	TOT	Andreae et al.[53]
Beijing, China	Nov. 2005 - Oct. 2006	6.9	0.0035 (winter)/ 0.0058 (summer)	TOT	Han et al.[28]
Beijing, China (roadside)	Aug. and Dec. 2009	12.3-17.9	0.0052 (day, summer) 0.0090 (night, summer) 0.0047 (day, winter) 0.0066 (night, winter)	Light absorption	Song et al.[31]
Hyderabad, India	January 2004	1.5-11.2	0.0073	Light absorption	Latha et al.[64]
Fort Meade, Maryland, USA	July 1999 – July 2000	0.7-1.2	0.0034	TOT	Chen et al.[25]
Baltimore, Maryland, USA	March – Nov. 2002	1.1	0.0023	TOT	Park et al.[26]
Mexico city, Mexico	April 2003/2005	-	0.0010	SP2	Baumgardner et al.[63]
Parque Morelos, Mexico	May – June 2010	2.2	0.0065	Light absorption	Shores et al.[30]
El Trompo, Mexico	June 2010	1.7	0.0050	Light absorption	Shores et al.[30]
Multiple sites, Europe	April/May/Sept 2008	-	0.0008-0.0062	SP2	McMeeking et al.[65]
Gwangju, Korea	**Dec. 2012 - Feb. 2013**	**2.4**	**0.0063 (day, winter) 0.0065 (night, winter)**	**Light absorption**	**This study**

Lists of Figure Captions

Figure 1. Location of BC measurement site in Gwangju
Figure 2. Temporal variations of (a) BC, and (b) $PM_{2.5}$ and SO_4^{2-} concentrations during study period
Figure 3. Diurnal cycles of (a) BC concentration, (b) CO concentration, (c) boundary layer height, (d) ambient temperature, (e) wind speed, and (f) ΔBC/ΔCO ratio for December, January, and February
Figure 4. Influence of wind speed on BC concentration
Figure 5. Influence of wind direction on BC concentrations. (a) All BC data at wind speeds > 1.0 m/s, (b) CPF plots for BC at 75% percentile
Figure 6. Relationships between BC and CO for daytime, nighttime, and two episodes. Slopes are in $\mu g/m^3$/ppb
Figure 7. Temporal variations of BC, wind speed, NO, and NOx, and relationship between NO/NO_x and CO/NO_x for two BC episodes
Figure 8. Temporal variations of SO_4^{2-}, NO_3^-, SOR and NOR for two BC episodes
Figure 9. PSCF results of BC for two BC episodes, A (left graph) and B (right graph)

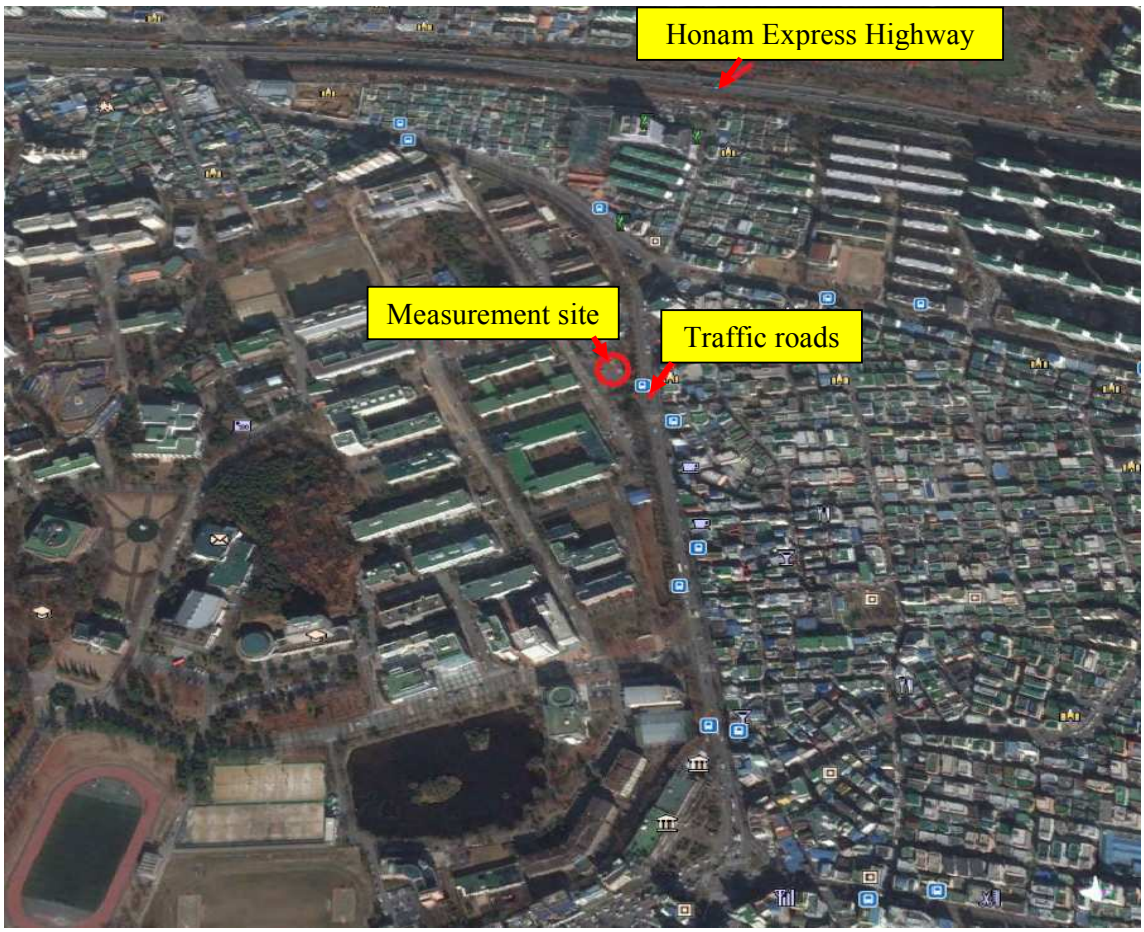

Figure 1. Location of BC measurement site in Gwangju

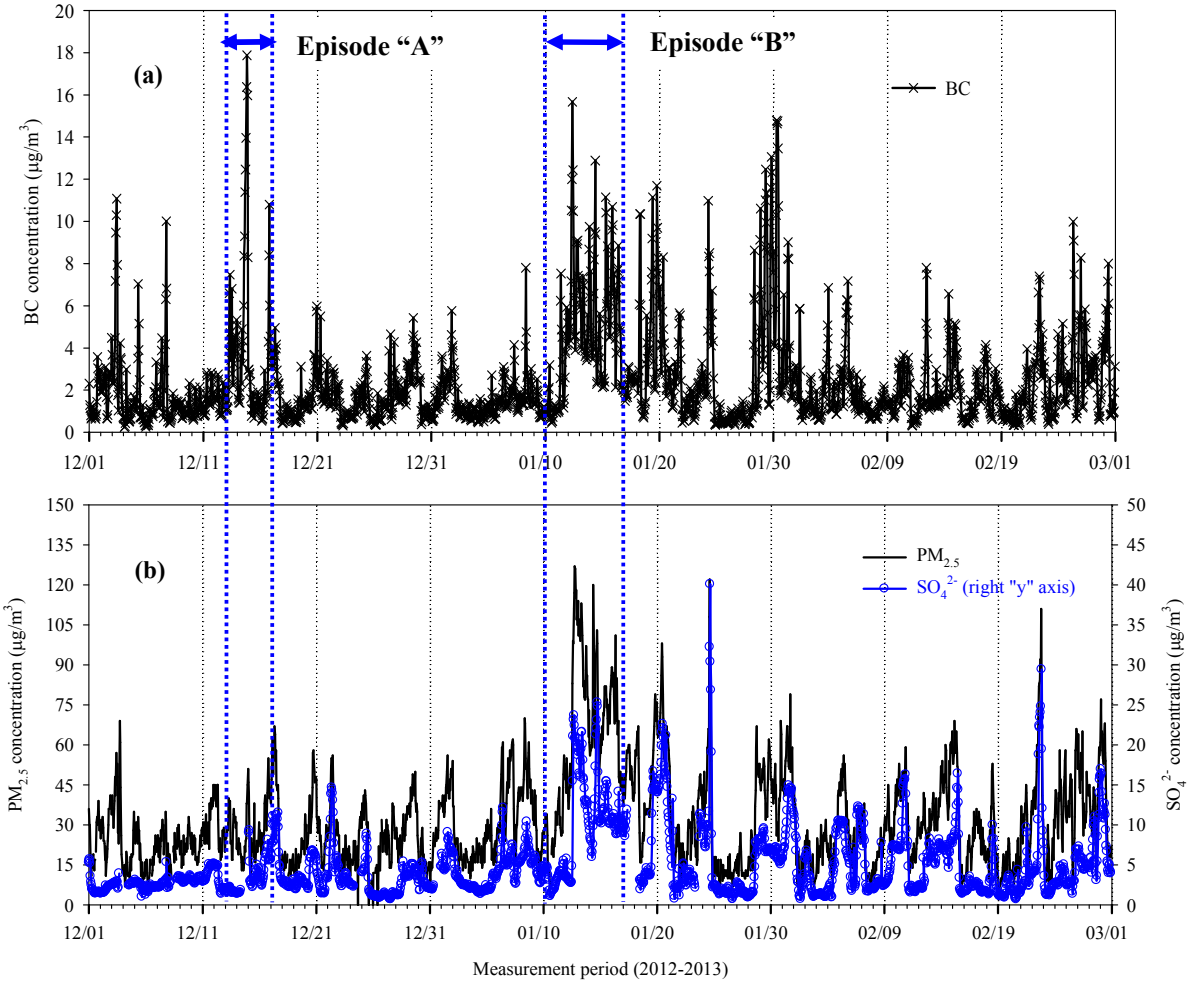

Figure 2. Temporal variations of (a) BC, and (b) $PM_{2.5}$ and SO_4^{2-} concentrations during study period

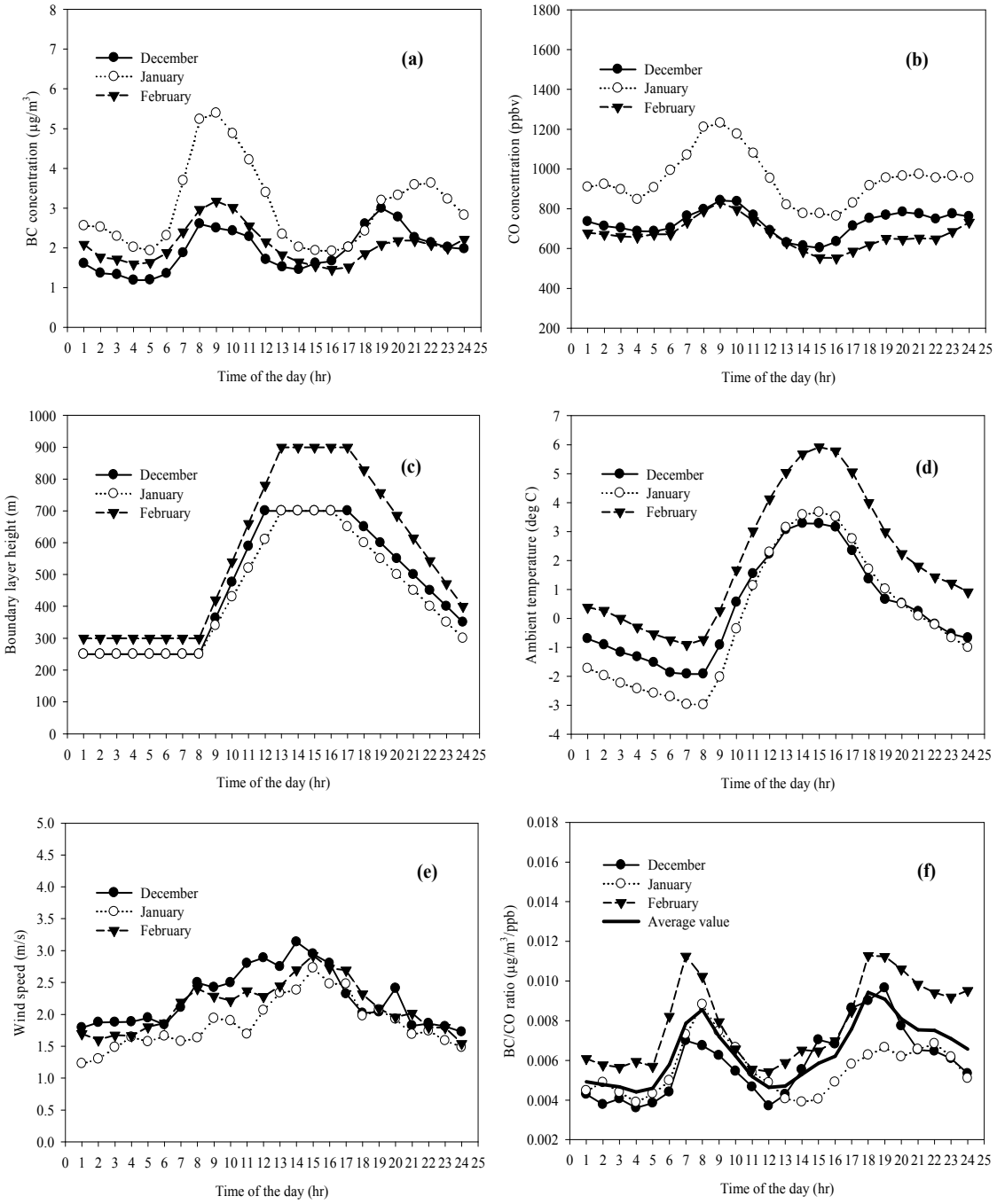

Figure 3. Diurnal cycles of (a) BC concentration, (b) CO concentration, (c) boundary layer height, (d) ambient temperature, (e) wind speed, and (f) ΔBC/ΔCO ratio for December, January, and February

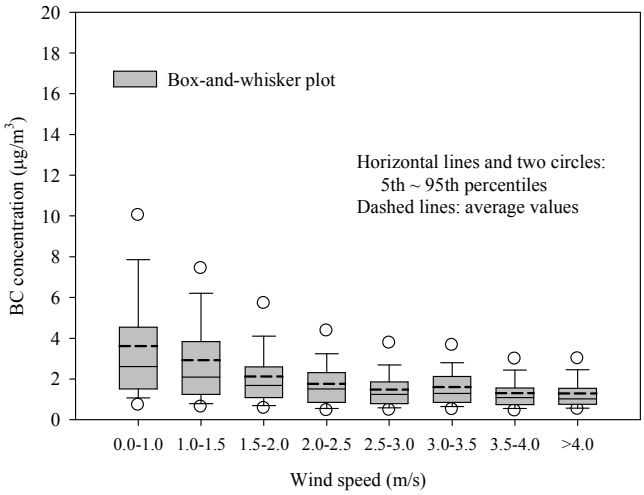

Figure 4. Influence of wind speed on BC concentration

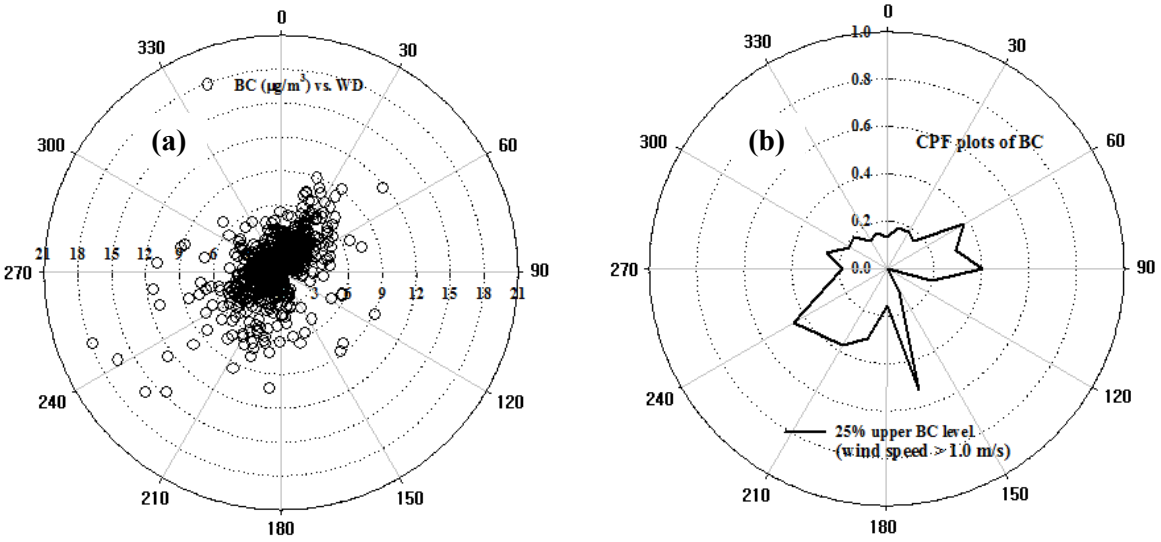

Figure 5. Influence of wind direction on BC concentrations. (a) All BC data at wind speed >1.0 m/s, (b) CPF plot for BC at 75% percentile

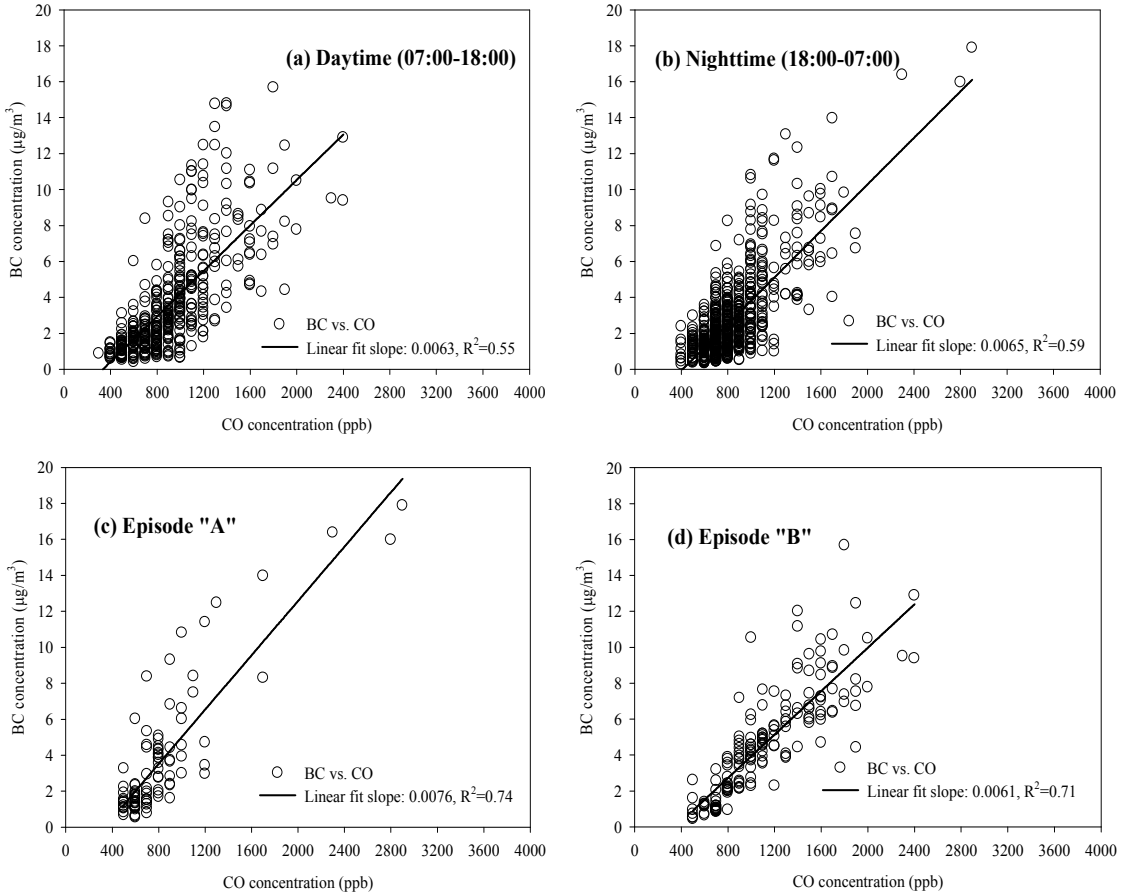

Figure 6. Relationships between BC and CO for daytime, nighttime, and two episodes. Slopes are in μg/m^3/ppb

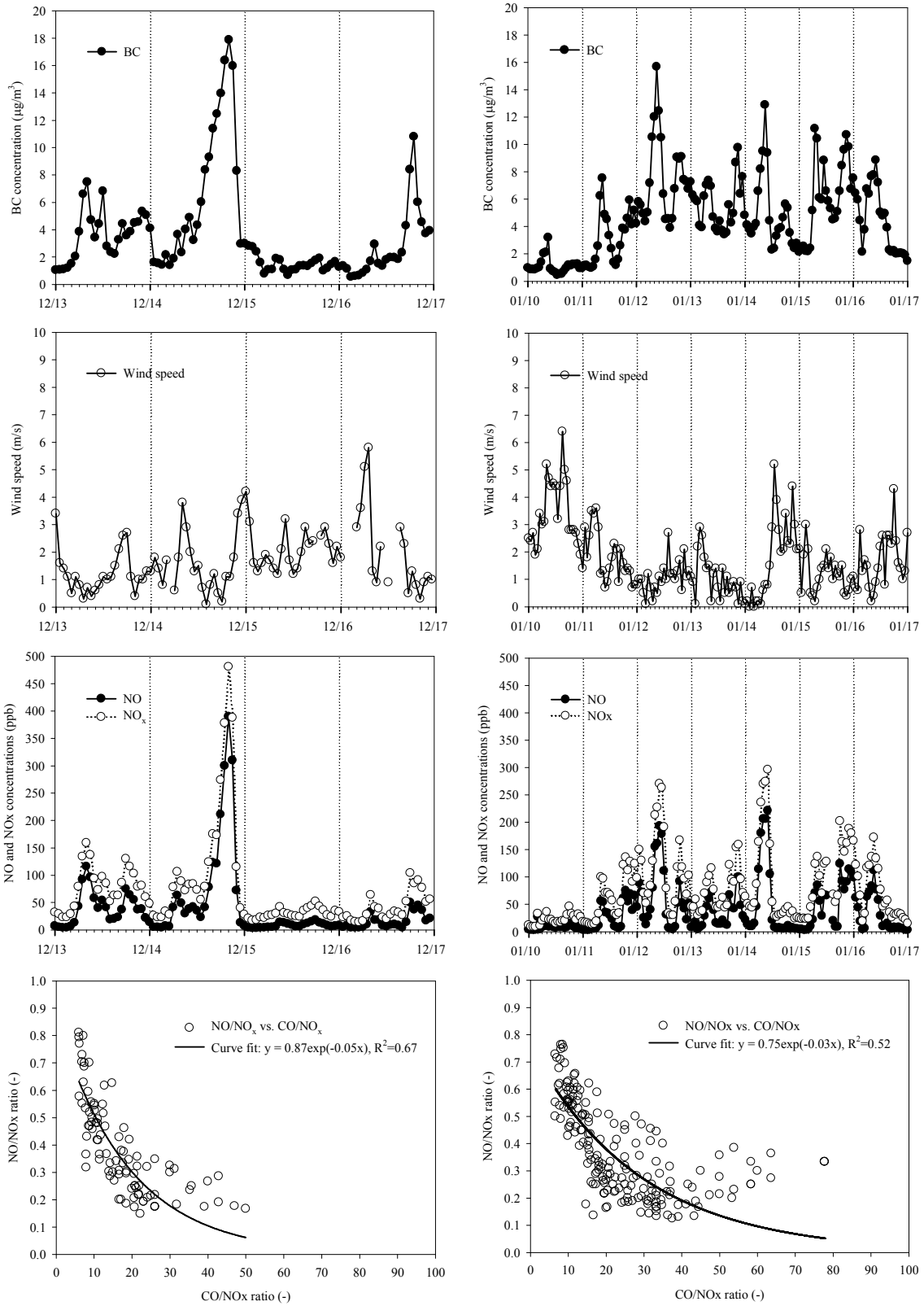

Figure 7. Temporal variations of BC, wind speed, NO, and NOx, and relationship between NO/NO_x and CO/NO_x for BC episode "A" (left graphs) and "B" (right graphs)

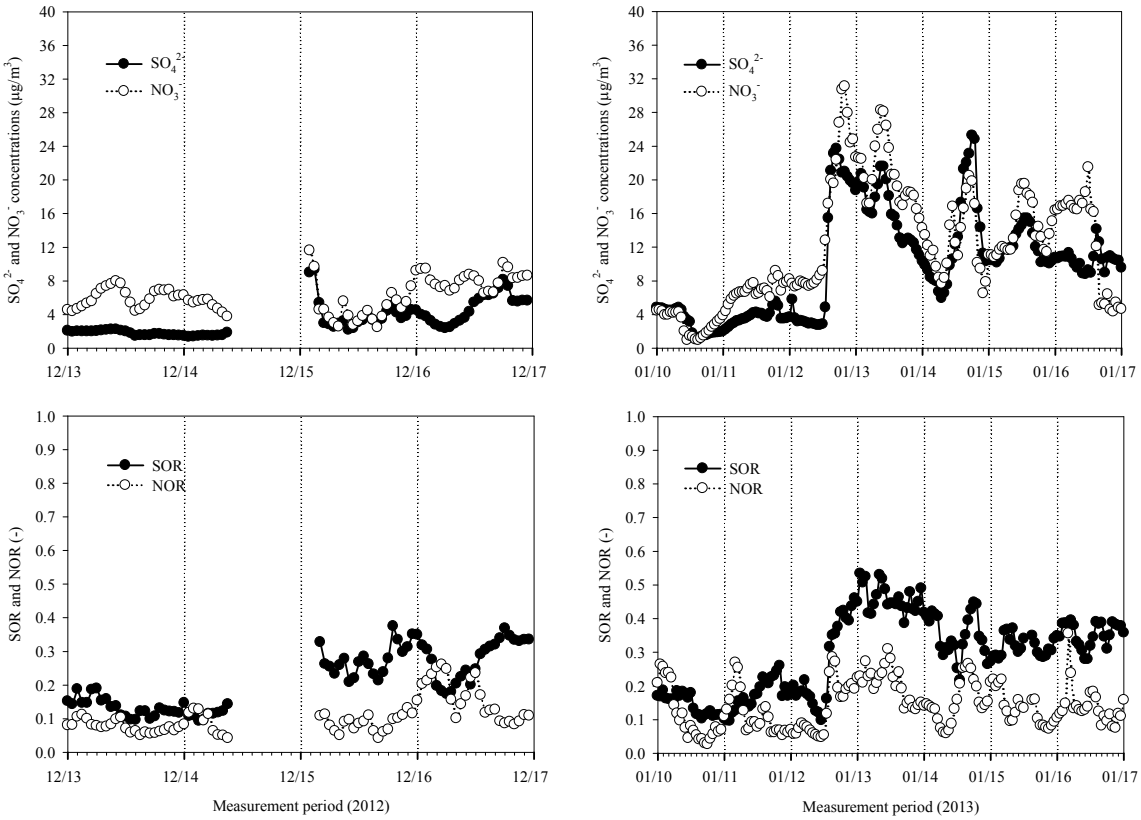

Figure 8. Temporal variations of SO_4^{2-}, NO_3^-, SOR and NOR for BC episode "A" (left) and "B" (right)

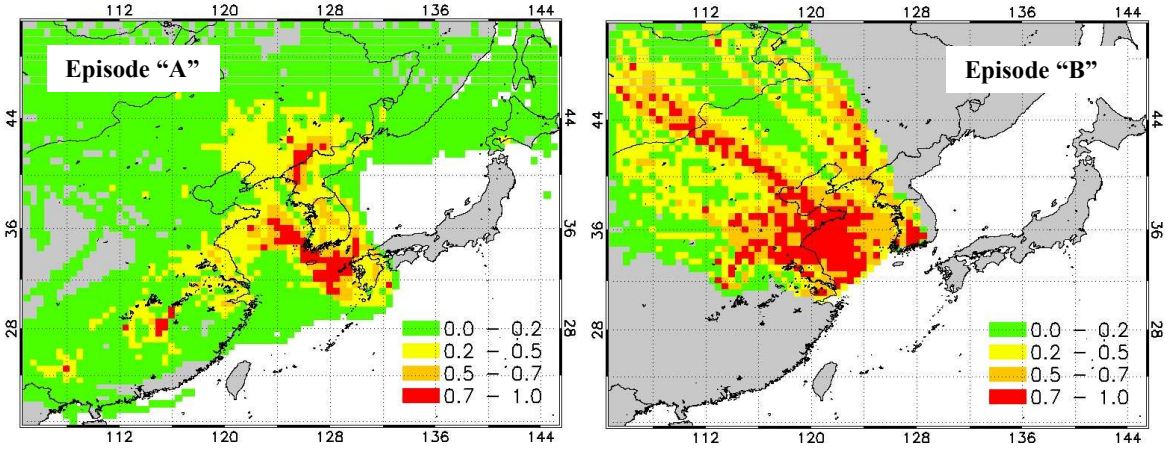

Figure 9. PSCF results of BC for two BC episodes, "A" (left graph) and "B" (right graph)